Ceramics International **22** (1996) 421–427

0272-8842(95)00131-X
0272-8842/96 $15.00 + .00

Interfaces in Continuous Filament Composites

R. J. Arsenault

Metallurgical Materials Laboratory, Department of Materials and Nuclear Engineering, University of Maryland, College Park, MD 20742-2115, USA

(Received 10 August 1995; accepted 16 October 1995)

Abstract: Interface structures in a continuous Al_2O_3 filament reinforced NiAl composite were investigated by transmission electron microscopy. There appeared to be an intimate bond between the NiAl matrix and the Al_2O_3 filaments. Simulation of TEM diffraction contrast images based upon a three dimensional finite element analysis was employed to investigate the nature of the residual strains in regions along the interface. The simulations suggested that radial residual strains within the Al_2O_3 filaments were randomly distributed along the interface. These strains were believed to be related to dislocation nucleation in the NiAl which results from the relaxation of the thermally generated residual stresses. © 1996 Elsevier Science Limited and Techna S.r.l.

1 INTRODUCTION

The use of continuous filaments as composite reinforcements is currently being considered as a means of improving the creep resistance of intermetallics, and there are a lot of examples but at present only a specific case will be considered. In particular, it has been demonstrated that single crystal Al_2O_3 filaments are capable of improving both the creep and fatigue resistance of NiAl.[1] The interfacial bond strength, which is strongly dependent upon the processing methods, plays a key role in the control of the mechanical properties of these continuously reinforced composites.[1] The strength of the interfacial bond is important because it strongly influences the thermal residual stresses (TRS) which develop during cooling caused by the coefficient of thermal expansion (CTE) mismatch between the filaments and the matrix. In a previous investigation[2] it was found that if an Al_2O_3 /NiAl composite with an as-fabricated interfacial bond strength (measured by push-out testing) in the range of 90–180 MPa was thermally cycled ten times in a temperature range of 373–1373 K, matrix cracking occurred. However, cracks were not observed after identical thermal cycling in those samples which had an interfacial bond strength in the range of 35–120 MPa. Also, the interfacial bond strength of these weakly bonded samples dropped to 5–30 MPa in the post thermal cycled condition. The mechanism responsible for the difference in interfacial bond strength is due to interfacial graphite islands.[3] It was also confirmed that the NiAl matrix was plastically deformed as a result of the relaxation of the TRS. Although dislocation densities in the region adjacent to the interface were found to be very high, dislocation generation in the interface region was not necessarily related to the interfacial bond strength since dislocation activity was observed in both weakly and strongly bonded composites.

An electron microscopy investigation was undertaken to determine the interface structures of the single crystal Al_2O_3 filament reinforced NiAl composites. Simulations of TEM diffraction contrast images based upon a three dimensional (3D) finite element method (FEM) analysis were generated to understand the residual strain at regions adjacent to the interface.

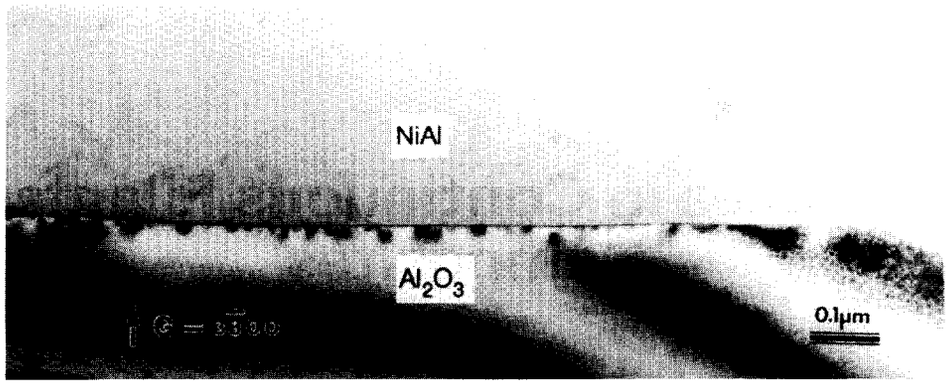

Fig. 1. TEM image of a clean interface between the single crystal Al_2O_3 filament and NiAl matrix after ten thermal cycles, inhomogeneous diffraction contrast is observed along the interface on the Al_2O_3 filament side.

2 MATERIALS AND EXPERIMENTAL METHODS

The composites used in this investigation consisted of a stoichiometric NiAl matrix unidirectionally reinforced with six layers of 125 μm diameter, *c*-axis oriented, continuous, single crystal Al_2O_3 filaments comprising 30 vol% of the composite, the matrix was fabricated from 50–150 μm diameter vacuum atomized pre-alloyed powders obtained from Homogeneous Metals, Inc., Clayville, NY. The Al_2O_3 filaments were supplied by Saphiton Inc., Milford, CT. The composites were fabricated using the powder–cloth (P–C) technique.[4] The composites were annealed at 1473 K for 4 h followed by furnace cooling. TEM samples of monolithic NiAl were produced via the dimple grinding plus an electro-polishing method. Polishing was performed in a solution of 5% perchloric acid + ethanol at ~253 K with an applied voltage of 50–70 V. The cross-section Al_2O_3/NiAl TEM samples were prepared by dimple grinding plus ion milling as described elsewhere.[5]

TEM and X-ray energy dispersive spectra (EDS) analyses were performed on a JEM 2000-FX analytical electron microscope equipped with Noran Voyager system. The foil thickness used in the calculation of the diffraction contrast image was measured by the convergent beam electron diffraction (CBED) method.[6,7] An ABAQUS FEM software package was used to simulate the interface strains. The programs used for diffraction contrast simulation of TEM images were written in Interactive Data Language (IDL) running on a Sun work station system.

Fig. 2. HREM image of the very thin area in Fig. 1.

3 EXPERIMENTAL RESULTS

There were no consistent crystallographic orientation relationships between the filaments and matrix, i.e. the orientations between the filament and matrix were random as shown in Fig. 1. Neither coherent nor semicoherent interfaces were observed between the filament and matrix. However, HREM investigations of the clean interface indicated that the matrix and filament formed direct contact without a noticeable intermediate layer or precipitates, as shown in Fig. 2. It is likely that a randomly direct bond between the Al_2O_3 filament and the NiAl matrix has been achieved on an atomic level at the clean interface.

An unusual observation is that diffraction contrast in the Al_2O_3 filament at the interface was not homogeneous, but rather modulated randomly along the clean interface, as shown in Fig. 1. The wavelength of the modulation is around 0.1 μm. The modulated diffraction contrast disappeared in regions where the foil thickness became less than a two-beam extinction distance with operating diffraction vector of $g = 3\bar{3}00$, which is less than

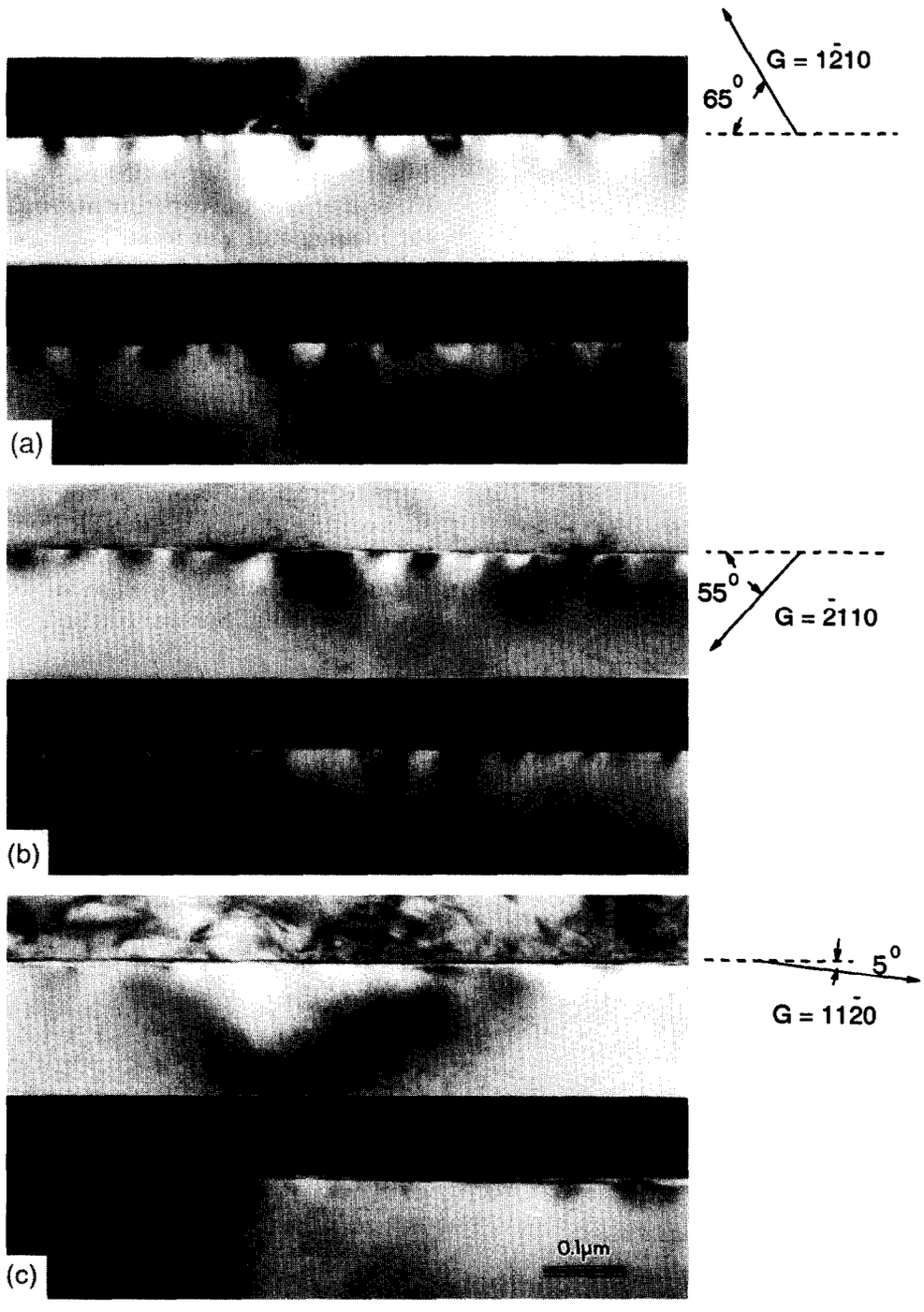

Fig. 3. TEM image of a clean interface between the single crystal Al_2O_3 filament and NiAl matrix after ten thermal cycles, (a)–(c) bright (top) and dark (bottom) field images of the interface with different operating diffractions, $t = 1.3\xi_g$ with $g = 110$.

95 nm. Different operating diffraction conditions were applied to produce different two-beam diffraction contrast images of the interface area, as shown in Fig. 3(a)–(c). According to an analysis of these images, two important features were observed. First, minimum diffraction contrast was obtained when the diffraction vector was almost parallel to the interface (Fig. 3(c)); second, the shape of the dark and bright areas of the image always tended to parallel the diffraction vector (Fig. 3(a) and (b)). Since there is no precipitation or any other second phase present in this interface region, it is likely that this modulated diffraction contrast is caused by an inhomogeneous distribution of strains which originate at the interface. Also, there was no indication of any interfacial dislocations.

4 MODELLING

To investigate the possible role of interfacial strain on the modulating diffraction contrast described above, an FEM analysis was undertaken to simulate various strain conditions originating from the interface. From these results TEM diffraction contrast images were then calculated and compared to the observed images.

Since the exact distribution of the randomly modulated strain is unknown, the goal of the current modelling was to reveal the basic character of these inhomogeneous strains along the interface. Comparison was made between the calculated images and the experimental images to see if the main important features of the experimental images described above could be duplicated by a number of simplified models. As shown in Fig. 4, the inhomogeneity of the strains was simulated as concentrated loads or surface tractions which were applied at the interface in an area with a dimension less than an extinction distance (ξ_g). This thickness was chosen since the foil thickness of the region in Fig. 1 was ~ 220 nm, which is $\sim 1.3\xi_g$ of $g = 11\bar{2}0$. To best fit into the experimental images, the size of the loading area was found to be ~ 50 nm.

Several possible loading configurations were examined. First, a concentrated pure shear load was considered, as shown in Fig. 4(a). The TRS has been partially relaxed as a result of the TEM sample preparation, i.e. the matrix material has been partially removed from the filament surface which could cause a shear stress at the remaining interface region. Second, a normal load was considered, Fig. 4(b), since the TRS will also be in the normal direction if it is not completely relaxed. Figure 4(c) presents a case of both shear and normal loading. Surface traction, Fig. 4(d), might

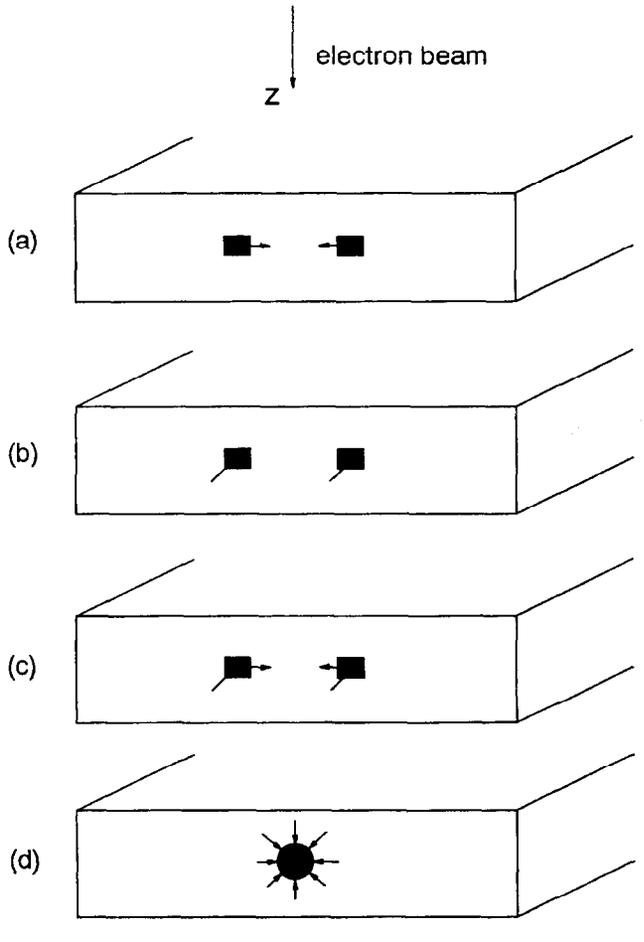

Fig. 4. Schematic illustrations of FEM models of strains introduced at interface, (a) concentrated shear load, (b) concentrated normal load, (c) both the shear and the normal loading, and (d) surface traction.

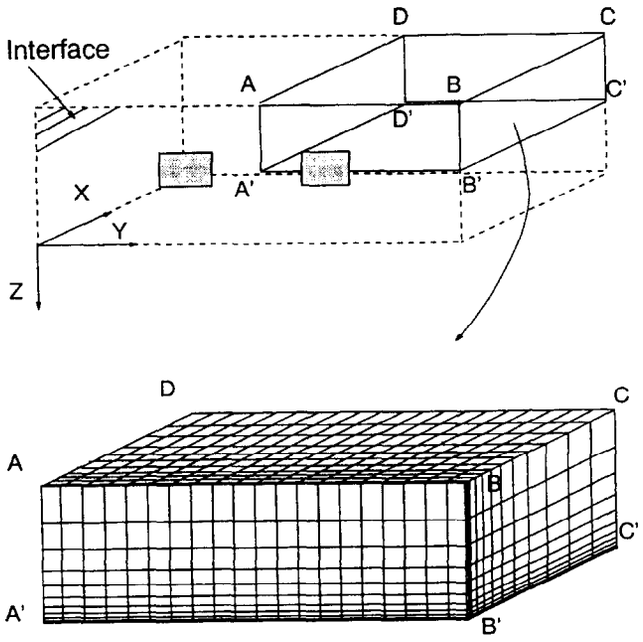

Fig. 5. An example of the FEM mesh where the 3D 8-node linear solid elements were used in all the FEM analyses. See Table 1 for boundary conditions.

also be developed during the sample cooling process, if the bond strength of the interface was not homogeneous.

The FEM analyses employed a three dimensional (3D) eight-node linear solid element and a displacement boundary condition which gave rise to a maximum strain of ~ 0.001 at the boundary to produce the observed diffraction contrast level. A maximum strain of 0.001 was used throughout the calculations (the corresponding maximum stress was ~ 200 MPa in the Al_2O_3). The diameter of the Al_2O_3 filament is so big (125 μm) that the interface can be approximated as a flat plane on a one-micron scale. According to symmetry, a quarter of the block was considered in all the FEM analyses. An example of the FEM mesh is shown in Fig. 5. Because of the nature of thin foils used as TEM samples, the boundary conditions of the FEM block were chosen so that the top and bottom surface (plane ABCD in Fig. 5) of the block were free of restrictions, as was the side plane BB'C'C. Following the symmetry requirement, plane AA'D'D and A'B'C'D' were restricted to move in the Y and Z directions, respectively. The interface, which is represented by the plane of ABB'A', had no restrictions whenever there is a normal loading at interface as the boundary condition. In the case of pure shear or surface contraction as the boundary condition, the interface was restricted in the X direction. The plane CC'D'D is totally restricted in the X, Y and Z directions because very thin regions of the Al_2O_3 filament in the TEM foils are present only in the vicinity of the interface, i.e. the foil thickness soon becomes very thick in the direction towards the centre of the filament. Subjected to these boundary conditions, stresses and strains obtained from the FEM analyses are rather localized around the loading area while the top and bottom surface are stress free. Stresses and strains near plane CC'D'D and plane BB'C'C are about 1–2 orders of magnitude smaller than the region close to the loading area. A more elaborate model which includes periodic boundary conditions on the plane of BB'C'C and the matrix constraint is currently being carried out.

Simulations of diffraction contrast images are based on the dynamical theory of diffraction contrast in the form developed by Howie and Whelan.[8] When two-beam conditions are applied, the amplitude of the transmitted and diffracted beams, i.e. A_0 and A_g, is determined by,

$$\frac{dA_O}{dz} = -\pi a A_0 + \pi(i - a')A_g$$

$$\frac{dA_g}{dz} = -\pi(i - a')A_0 + \pi(-a - 2i(w + \beta'))A_g$$

where

$$\beta' = \frac{\mathrm{d}(g.u)}{\mathrm{d}z}$$

In these equations, the depth (z) is normalized by the two-beam extinction distance (ξ_g), g is the operating diffraction vector, w is a dimensionless form of the deviation parameter, and u is the displacement field within the sample which causes the diffraction contrast. In the current investigation, u was obtained from the FEM analyses, i.e. the simulated diffraction contrast image was based on the displacement field generated from the FEM analyses. The effect of inelastic scattering was treated phenomenologically by absorption parameters a and a', where a is the exponential decay parameter and a' represents the anomalous absorption. As suggested by Hashimoto *et al.*,[9] and generally adapted by many other investigators, $a = a' = 0.1$ was used in this investigation.

In the calculation of the diffraction contrast image, the whole FEM block was equally divided into 128×128 columns parallel to the electron beam direction. The total image size was 128×256 columns, which contains twice as many columns as the FEM block (Fig. 5). The advantage of using IDL in the programming is that an integration column-by-column can be avoided. The integration can be done in all the columns simultaneously by matrix operation, i.e. each of the variables in the equations can be represented by a 128×128 matrix. Integration of the equations started at $A_0 = 1$ and $A_g = 0$. At each integration step, the displacement matrix from the FEM analyses was inserted into these equations. Displacements between the FEM nodes were linearly interpolated from the nearest neighbour nodes. The integration was terminated at the desired foil thickness. The resulting diffraction contrast matrix was then normalized into a 256 gray level black and white image. Zero intensity was taken as complete darkness in all the simulated images.

The calculated TEM diffraction contrast images corresponding to the loading conditions depicted in Fig. 4 are shown in Fig. 6. These images were calculated using the same diffraction conditions and foil thickness as those of the experimental images (Fig. 1). It turns out that only the simple normal loading model (Fig. 6(b)) can duplicate all the major features of the experimental images. The contrast is localized around the loading area (in a range of ~ 0.1 μm from interface) which indicates that the residual strains are concentrated at that region. Furthermore, changes of the location of the loading area in the depth direction (z-direction) will not drastically change the basic features of the calculated diffraction contrast images.

5 DISCUSSION

The modulated diffraction contrast of the clean interface may be caused by an inhomogeneous distribution of normal residual strains along the interface. The difference in the coefficient of expansion between Al_2O_3 and NiAl is $0{\cdot}4\times10^{-6}$/K. The bond between Al_2O_3 filament and NiAl appears to be frictional in nature. The data obtained from the simulation indicates that the magnitude of the strain at the interface should be at least $\sim10^{-3}$ and localized around the interface in a range of ~0.1 μm. It is unknown why the normal residual strain would modulate along the interface and how it is exactly distributed. One possible reason is that because of the relaxation of TRS the plastic deformation in NiAl is not microscopically homogeneous, i.e. the dislocation generation in NiAl created an inhomogeneous 'back stress' towards the filament. Since the filament cannot be plastically deformed, this back stress will build up a considerable elastic strain in the filament. One supporting observation is that the modulated diffraction contrast does disappear in

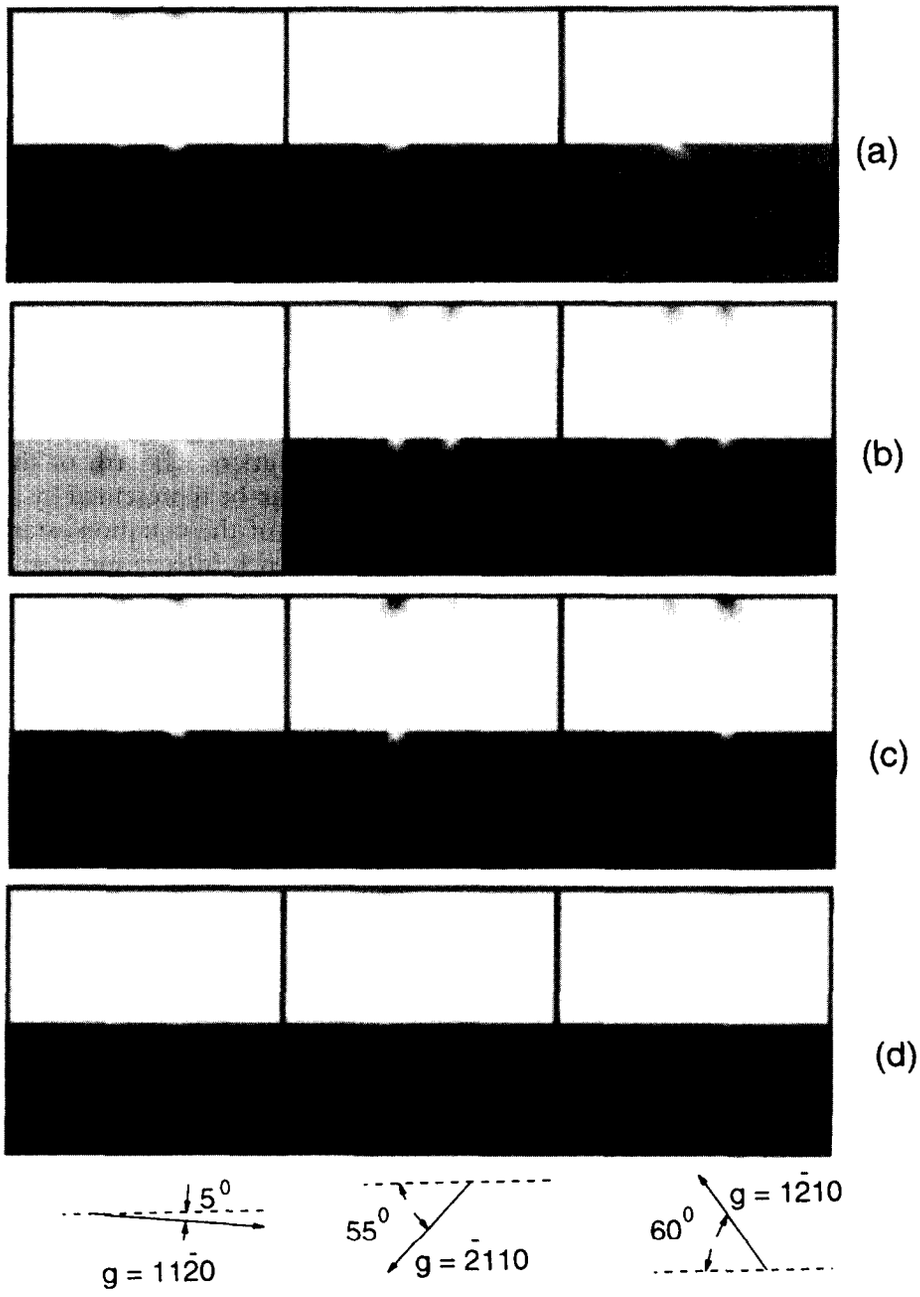

Fig. 6. Bright field (top) and dark field (bottom) diffraction contrast image simulations of the FEM model under different diffraction conditions, $w=1.0$ and $t=1.3\xi_g$: (a) concentrated shear load, (b) concentrated normal load, (c) both shear and normal, and (d) surface traction.

very thin area (less than ~90 nm), i.e. the edge of perforation hole of the TEM sample, where dislocations have escaped from the foil in that area.

Semicoherent interfaces between Al_2O_3 and NiAl have been observed in a XD-processed TiB_2/NiAl composite which contained Al_2O_3 particles. In that system low indexed crystallographic planes of both α-Al_2O_3 and NiAl were aligned.[10] The current investigation does not rule out the possibility of the existence of a semicoherent interface between the Al_2O_3 and NiAl, but none were observed. One important difference between the XD-processed TiB_2/NiAl composite and the current composite is that in the current composite dislocation generation due to TRS has occurred. This dislocation generation was not observed in the XD-processed TiB_2/NiAl composite. In general, plastic deformation by dislocation motion is considered microscopically inhomogeneous and therefore modulation of strains is expected to occur in all regions of the ceramic–metal interface where the metal phase undergoes plastic deformation and the ceramic phase remains elastic.

6 CONCLUSIONS

From the data generated in the present investigation, the following conclusions can be drawn.

The matrix and filament bonded without any noticeable intermediate layer or precipitates. It is likely that a random direct bond between Al_2O_3 filaments and NiAl matrix was achieved at an atomic level at the clean interfaces. Modulating diffraction contrast along the interface suggest that radial residual strains within the Al_2O_3 are inhomogeneously distributed along the interface. It is believed that the random modulation of the radial residual strains in the Al_2O_3 filament along the interface is caused by plastic deformation of the NiAl matrix.

ACKNOWLEDGEMENTS

The author wishes to acknowledge the assistance of Drs L. Wang and R. R. Bowman and Mr K. Xu. He also wishes to acknowledge the continuing support of Dr S. Fishman of the Office of Naval Research. The work was supported by the Office of Naval Research under grant N00014-94-10118.

REFERENCES

1. BOWMAN, R. R., In *Intermetallic Matrix Composites II, Proc. Materials Research Society Symp. Vol. 273*, ed. D. B. Miracle, D. L. Anton & J. A. Gravees. Materials Research Society, Pittsburgh, PA, 1992, p. 145.
2. WANG, L., BOWMAN, R. R. & ARSENAULT, R. J., to be published.
3. WANG, L., XU, K., BOWMAN, R. R. & ARSENAULT, R. J., *Metall. Trans.*, **26A** (1995) 897.
4. PICKENS, J. W., NOEBE, R. D., WATSON, G. K., BRINDLEY, P. K. & DRAPER, S. L., NASA Technical Memorandum 102060, 1989.
5. ARSENAULT, R. J., WANG, L. & FENG, C. R., *Acta Metall. Mater.*, **39** (1991) 47.
6. ALLEN, S. M., *Phil. Mag.*, **A43** (1981) 325.
7. KELLY, P. M., JOSTSONS, A., BLAKE, R. G. & NAPIER, J. G., *Phys. Stat. Sol.*, **A31** (1975) 771.
8. HOWIE, A. & WHELAN, M. J., *Proc. Roy. Soc.*, **A263** (1962) 217.
9. HASHIMOTO, H., HOWIE, A. & WHELAN, M. J., *Phil. Mag.*, **5** (1960) 967.
10. WANG, L. & ARSENAULT, R. J., *Metall. Trans.*, **22A** (1991) 3013.